

Electronic Supporting Information: *Transition to elasto-capillary thinning dynamics in viscoelastic jets* by Konstantinos Zinelis, Thomas Abadie, Gareth H. McKinley, and Omar K. Matar

Three-dimensional disturbances in a viscoelastic jet

In the Supplementary Information, we study the development of asymmetric disturbances in a viscoelastic jet. In order to confirm that axisymmetry prevails in the jetting configurations studied in the main text, two-dimensional (2D) axisymmetric simulations are compared with three-dimensional (3D) computations. The 3D simulations have been carried out using the same numerical framework, *Basilisk*, used to generate the results in the original version of the paper.

There is abundant literature regarding the development of axisymmetric and asymmetric disturbances during jet formation in polymeric fluids. The experimental studies of [Ghafourian et al. \[1991\]](#), [Mayer and Branam \[2004\]](#), [Lefebvre and McDonell \[2017\]](#) have demonstrated the development of asymmetric disturbances. Theoretical work has also shown the critical role of fluid inertia (characterised by the Weber number $We = \rho U_{jet}^2 R_0 / \gamma$), the gas-liquid density ratio (ρ_g / ρ_l), the viscosity (characterised by the Ohnesorge number $Oh = \eta_l / \sqrt{(\rho R_0 \gamma)}$), and the fluid elasticity (expressed through either the intrinsic Deborah number $De = \tau / \sqrt{\rho R_0^3 \gamma}$ or Elasticity number $El = \tau \eta_l / (\rho R_0^2)$) [[Liu and Liu, 2006](#), [Ruo et al., 2011](#), [Yang et al., 2013](#), [Ding et al., 2022](#), [Deng et al., 2023](#), [Liu et al., 2023](#)]. These works also highlight the effect that an un-relaxed elastic tension can have on the viscoelastic jet instability, and more recently, there have been also studies that investigated more complex cases where the air-swirl and the effect of co-axial flow were considered. The work of [Ruo et al. \[2008\]](#) and [Liu and Liu \[2008\]](#) (who studied the case of viscoelastic jets) showed that the asymmetric modes are caused by the aerodynamic interactions and become dominant for high Weber ($We > 10^3$), gas-to-liquid density ratios ($\rho_g / \rho_l > 10^{-1}$), and Deborah ($De > 10$) numbers. In comparison to these thresholds, we note that the range of parameters studied here ($We = 8, 16, 36, De = 1, Oh = 0.2, \rho_g / \rho_l = 0.01$ [[Turkoz et al., 2018, 2021](#)]) the associated flows are expected to remain axisymmetric.

In the present simulations (2D axisymmetric and 3D), the flow upstream of the nozzle exit plane is not taken into consideration; instead, the inlet boundary condition for the axial velocity component is a uniform dimensionless velocity profile of the jet U_{jet} with an imposed

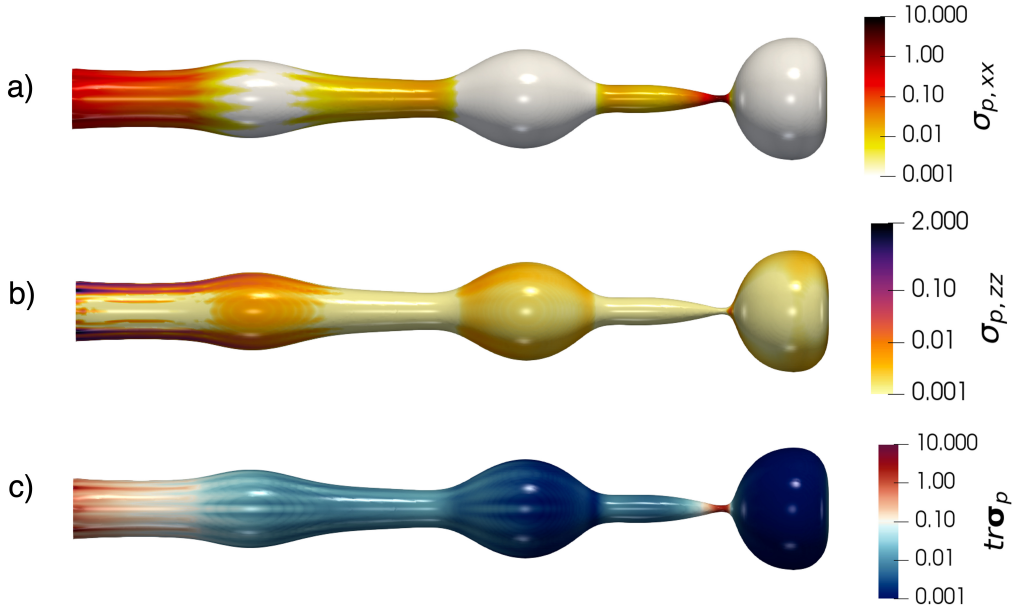


Figure S1: Three-dimensional contour plots of a) the axial polymeric stress component $\sigma_{p,xx}$, b) the tangential polymeric stress component $\sigma_{p,zz}$, and c) the trace of the polymeric stress tensor $tr\sigma_p$, in a viscoelastic jet at $We = 16$, $\epsilon_u = 0.15$ and $LVL = 11$. All other simulation parameter values are the same as in Table 2 in the main text.

perturbation described by:

$$U_{jet} = \sqrt{We} \left(1 + \epsilon_u \sin(\sqrt{We} k t) \right), \quad (S1)$$

where $\epsilon_u = 0.15$ is the amplitude of the imposed perturbation on the velocity of the jet and k is the dimensionless wavenumber. The maximum level of refinement achieved in the three-dimensional simulations is $LVL = 11$, which corresponds to a minimum grid-cell size $\Delta x = \Delta y = \Delta z \approx 0.05$. Here, we do not resolve down to very small lengths as was done in the paper ($\Delta x \approx 0.006$), as the main focus is the initial jet deformation which leads to the formation of the viscoelastic thread and whether asymmetric flows develop and dominate the dynamics.

We first present in Figure S1 3D contour plots of the axial polymeric stress component $\sigma_{p,xx}$, the tangential polymeric stress component in the third dimension $\sigma_{p,zz}$, and the trace of the polymeric stress tensor $tr(\sigma_p) = \sigma_{p,xx} + \sigma_{p,yy} + \sigma_{p,zz}$. For the 3D simulations, (x, y, z) correspond to the streamwise, spanwise, and vertical directions, respectively. We first observe the development of high axial stress values close to the nozzle which subsequently relax as we move downstream before going through a steep increase up to values of the order of 10s inside the formed viscoelastic thread that connects the leading droplet with the rest of the liquid jet. In addition, we detect the development of considerable tangential elastic stresses in the z -direction

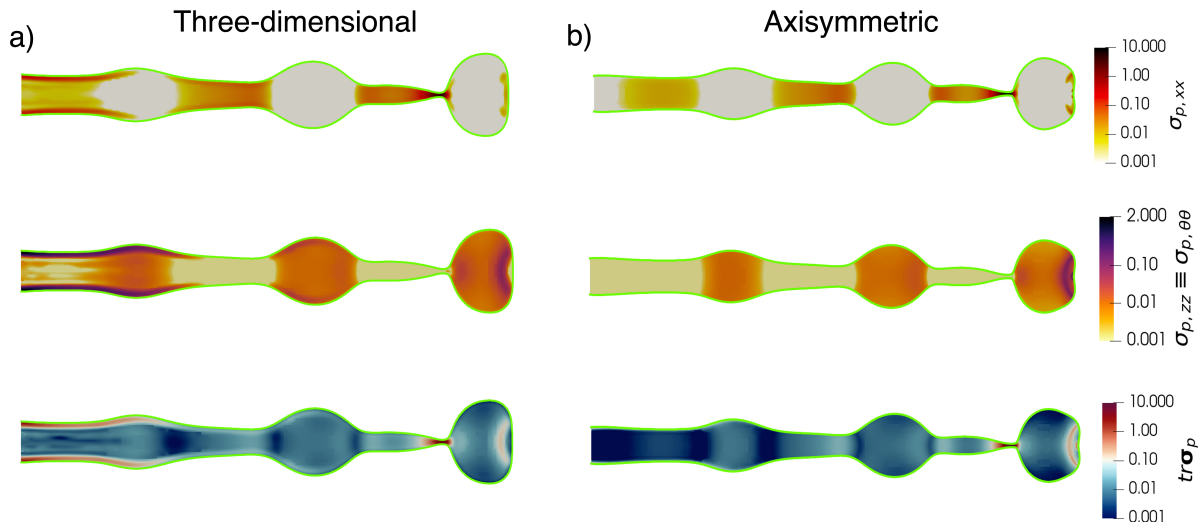


Figure S2: Two-dimensional (2D) contour plots in a viscoelastic jet obtained from a) fully 3D simulations (at $z=0$) at $We = 16$, $\epsilon_u = 0.15$ and $LVL = 11$ and b) axisymmetric simulations at $We = 16$, $\epsilon_u = 0.15$ and $LVL = 14$ of the axial elastic stress component $\sigma_{p,xx}$, the azimuthal elastic stress component $\sigma_{p,\theta\theta}$ (here $\sigma_{p,zz}$ coincides with $\sigma_{p,\theta\theta}$) and the trace of the elastic stress tensor $tr(\sigma_p)$. All other simulation parameter values are the same as in Table 2 in the main text.

close to the inlet which are seen to completely decay downstream of the inlet. This can also be seen from the contour plot of the trace of polymeric stresses where we see that as we move away from the inlet and approach the pinch-off region, the main contribution comes from the axial elastic stress component. These results provide evidence that the emergent 3D jet profiles for the parameters chosen in our paper are indeed axisymmetric.

To validate this observation, we compare in Figure S2 two-dimensional (2D) contour plots of 2D slices in the plane $z = 0$ of the 3D simulations in Cartesian coordinates (x, y, z) against the results of the simulations presented in the manuscript in axisymmetric coordinates (r, θ, x) . In this plane, the tangential polymeric stress component in the third direction $\sigma_{p,zz}$ corresponds to the azimuthal stress component $\sigma_{p,\theta\theta}$ in the axisymmetric coordinate system. In addition, $\sigma_{p,xx}$ is the axial polymeric stress component in both coordinate systems. Figure S2 shows that the stresses in the axisymmetric simulations attain slightly higher maximum values than those in the 3D simulations and the length of the jet of the 3D simulations is slightly shorter than the axisymmetric jet (around $\approx 1R_0$). This can be explained as a result of the higher spatial resolution achieved in the axisymmetric simulations.

Overall, as also seen in Figure S1, the axial polymeric stress component starts from high values close to the inlet, then relaxes to zero inside the formed beads, while it becomes the critical component for the stabilisation of the viscoelastic thread before the final pinch-off. On

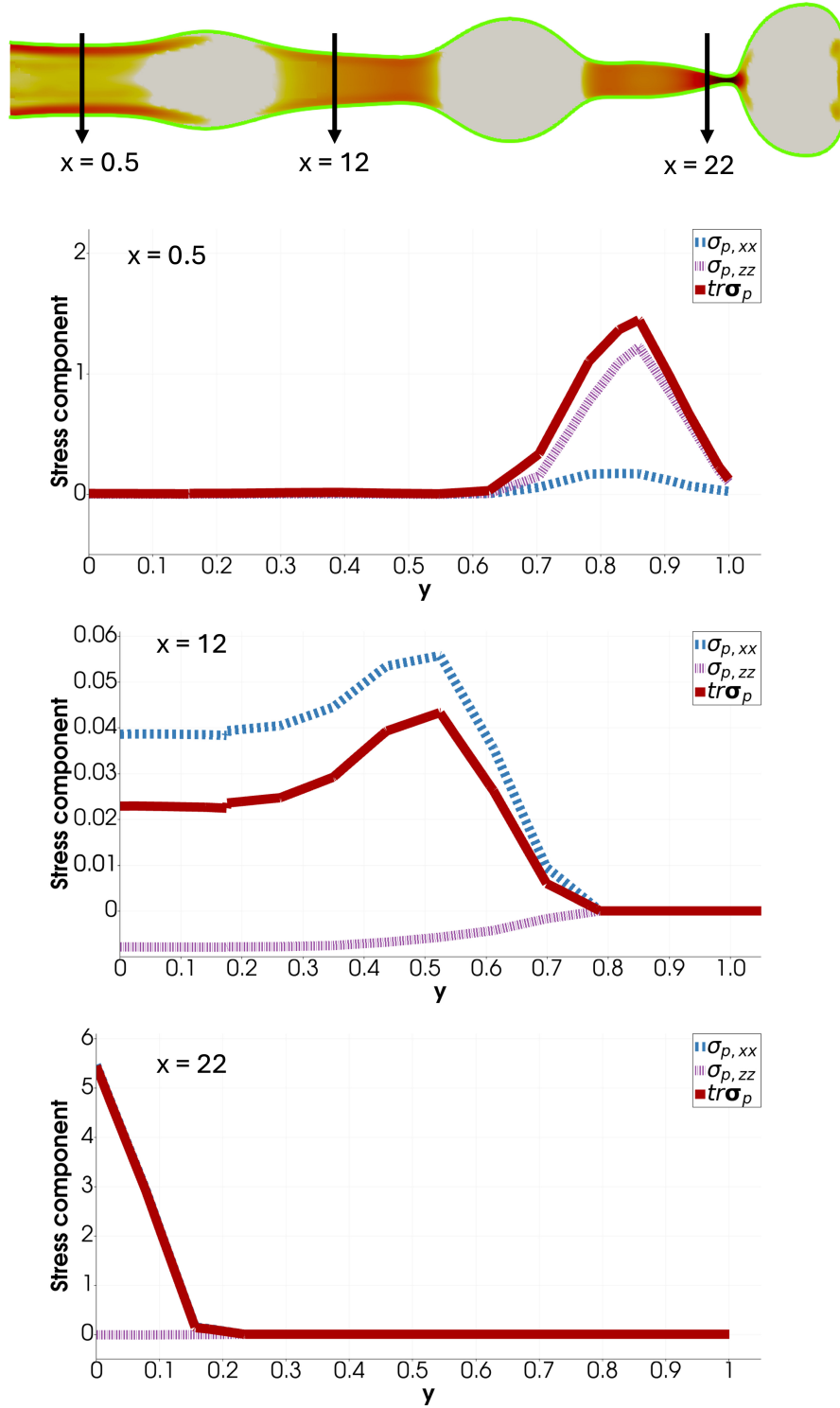


Figure S3: 2D contour at $z = 0$ of the axial polymeric stress component in a 3D viscoelastic jet at $We = 16$, $\epsilon_u = 0.15$ and $LVL = 11$, and the radial profiles of the axial polymeric stress component $\sigma_{p,xx}$, the azimuthal polymeric stress component $\sigma_{p,\theta\theta}$ and the trace of the elastic stress tensor $tr(\sigma_p)$ obtained from 2D contours at three different axial locations $x = 0.5$, $x = 12$ and $x = 22$ along the jet. All other simulation parameter values are the same as in Table 2 in the main text.

the other hand, the azimuthal elastic stress in the 2D slices of the 3D simulation exhibits its maximum (≈ 2) at distances very close to the inlet, while this is not captured by the axisymmetric simulation. Nonetheless, we observe that developing azimuthal elastic stresses do not lead to asymmetric disturbances as we move away from the inlet where the jet morphology remains axisymmetric. As the contour plot of the trace of the stress shows, the axial elastic stress is clearly the dominant component which drives the beads-on-the-string morphology, the focus of our study.

In Figure S3, we also provide the radial profiles ($0 \leq y \leq 1$; in the 2D slices at $z = 0$, the Cartesian y -direction coincides with the radial coordinate of the axisymmetric framework) of the elastic stress components under consideration and the trace of the stresses at three fixed axial locations which represent a location close to the inlet ($x = 0.5$), mid-way from the inlet ($x = 12$) and at the formed viscoelastic thread ($x = 22$). In this figure, we see the high values of the azimuthal stress at the inlet which gradually decays at longer distances, while the axial elastic stress component decisively dominates after the location where the first bulge (approximately $x \geq 10$) is formed.

Finally, we also study the robustness of the axisymmetric assumption when swirl is imposed at the inlet in the 3D simulations. We achieve this by setting a non-zero dimensionless mean azimuthal velocity (here $U_\theta = 1$) at the inlet, following the same perturbation as in the axial velocity component described by Eq. (S1). In the Cartesian coordinates, this corresponds to two mean tangential velocity components $U_y = U_\theta z$ and $U_z = -U_\theta y$. In Figure S4, we provide the 2D contour plots at $z = 0$ obtained from the 3D simulations with swirl at the inlet. In addition to the axial and azimuthal elastic stress and the trace of the elastic stresses, we also show the contour plot of the tangential velocity component U_z which coincides in this plane with the azimuthal velocity U_θ . The axisymmetric results are highly robust even to those disturbances.

In summary, we show using fully 3D simulations that for the flow regime investigated in our work for a low-speed, weakly viscoelastic jet ($We \leq 36, Oh = 0.2, De = 1, \rho_g/\rho_l = 0.01$), the axisymmetric simulations adequately resolve and capture the thinning process as well as the transition to the critical elasto-capillary dynamics in a viscoelastic jet.

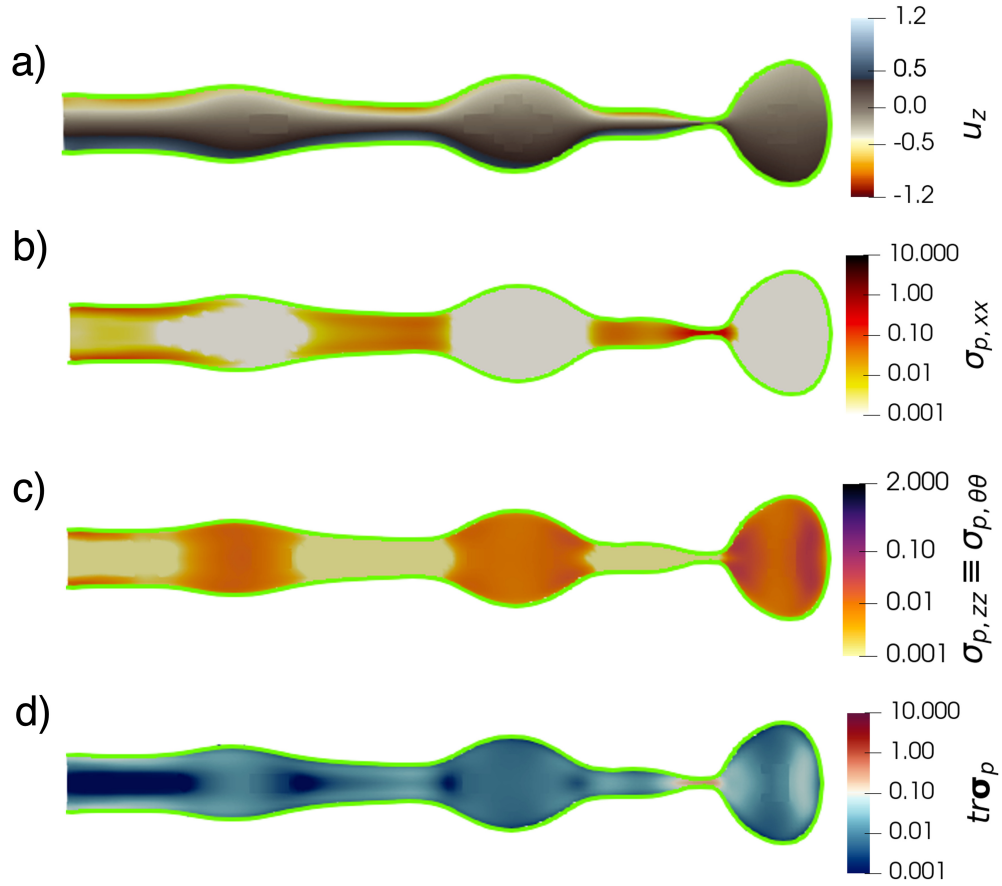


Figure S4: 2D contours at $z = 0$ in the 3D viscoelastic jet at $We = 16$, $\epsilon_u = 0.15$ and $LVL = 11$ with a swirl at the inlet with $U_\theta = 1$ of a) the tangential velocity u_z b) the axial polymeric stress component $\sigma_{p,xx}$, c) the tangential polymeric stress component $\sigma_{p,zz}$, and d) the trace of the polymeric stress tensor $tr\sigma_p$. All other simulation parameter values are the same as in Table 2 in the main text.

Bibliography

- X.-d. Deng, H.-r. Wang, X. Cui, B.-l. Shi, Y. Tang, and N.-f. Wang. Linear stability of viscoelastic confined liquid jet in the presence of gas velocity oscillations. *Physics of Fluids*, 35(6), 2023.
- Z. Ding, K. Mu, T. Si, and Y. Jian. Linear instability analysis of a viscoelastic jet in a co-flowing gas stream. *Journal of Fluid Mechanics*, 936:A6, 2022.
- A. Ghafourian, S. Mahalingam, H. Dindi, and J. Daily. A review of atomization in liquid rocket engines. In *29th Aerospace Sciences Meeting*, page 283, 1991.
- A. H. Lefebvre and V. G. McDonell. *Atomization and sprays*. CRC press, 2017.
- L. Liu, M. Yao, R. Dong, L. Qian, and Q. Fu. Unrelaxed tensile stress impacts on the instability of viscoelastic sheets with the gas velocity oscillation. *Physics of Fluids*, 35(2), 2023.
- Z. Liu and Z. Liu. Linear analysis of three-dimensional instability of non-newtonian liquid jets. *Journal of Fluid Mechanics*, 559:451–459, 2006.
- Z. Liu and Z. Liu. Instability of a viscoelastic liquid jet with axisymmetric and asymmetric disturbances. *International Journal of Multiphase Flow*, 34(1):42–60, 2008.
- W. O. H. Mayer and R. Branam. Atomization characteristics on the surface of a round liquid jet. *Experiments in fluids*, 36(4):528–539, 2004.
- A.-C. Ruo, M.-H. Chang, and F. Chen. On the nonaxisymmetric instability of round liquid jets. *Physics of Fluids*, 20(6), 2008.
- A.-C. Ruo, F. Chen, C.-A. Chung, and M.-H. Chang. Three-dimensional response of unrelaxed tension to instability of viscoelastic jets. *Journal of fluid mechanics*, 682:558–576, 2011.
- E. Turkoz, J. M. Lopez-Herrera, J. Eggers, C. B. Arnold, and L. Deike. Axisymmetric simulation of viscoelastic filament thinning with the Oldroyd-B model. *J. Fluid Mech.*, 851:1–13, 2018. ISSN 0022-1120. doi: 10.1017/jfm.2018.514.

E. Turkoz, H. A. Stone, C. B. Arnold, and L. Deike. Simulation of impulsively induced viscoelastic jets using the Oldroyd-B model. *J. Fluid Mech.*, 911:1–29, 2021. ISSN 14697645. doi: 10.1017/jfm.2020.1053.

L.-J. Yang, M.-X. Tong, and Q.-F. Fu. Linear stability analysis of a three-dimensional viscoelastic liquid jet surrounded by a swirling air stream. *Journal of Non-Newtonian fluid mechanics*, 191:1–13, 2013.